PHYSICAL REVIEW C **82**, 044318 (2010)

Systematics of one-quasiparticle configurations in neutron-rich odd Sr, Zr, and Mo isotopes with the Gogny energy density functional

R. Rodriguez-Guzman,[1] P. Sarriguren,[2] and L. M. Robledo[2,*]
[1]*Instituto de Estructura de la Materia, CSIC, Serrano 123, E-28006 Madrid, Spain*
[2]*Departamento de Física Teórica, Universidad Autónoma de Madrid, E-28049 Madrid, Spain*
(Received 26 July 2010; revised manuscript received 27 September 2010; published 29 October 2010)

The systematics of one-quasiparticle configurations in neutron-rich Sr, Zr, and Mo odd isotopes is studied within the Hartree-Fock-Bogoliubov plus equal filling approximation method preserving both axial and time-reversal symmetries. Calculations based on the Gogny energy density functional with both the standard D1S parametrization and the new D1M incarnation of this functional are included in our analysis. The nuclear deformation and shape coexistence inherent to this mass region are shown to play a relevant role in the understanding of the spectroscopic features of the ground and low-lying one-quasineutron states.

DOI: 10.1103/PhysRevC.82.044318 PACS number(s): 21.60.Jz, 21.10.Pc, 27.60.+j

I. INTRODUCTION

The theoretical description of odd-mass nuclei is a difficult task in mean-field models and, for that reason, they have been much less studied than the corresponding even-even systems although they roughly constitute half of the existing nuclides. The properties of odd nuclei are, however, relevant, for example, to understand odd-even effects related to pairing correlations, as well as to constrain nuclear energy density functionals (EDFs) aiming to reach a reasonable spectroscopic quality. Within this context, the energies, spins, and parities of the (neutron and/or proton) multiquasiparticle excitations are basic pieces of information to get insight into the underlying nuclear structure. Thus, the interest in the properties of odd-A nuclei and their computational challenges have been lately revived [1–5].

One of the main technical difficulties in the description of odd nuclei is that the (exact) blocking procedure [6,7] requires the breaking of time-reversal invariance making the calculations troublesome. Moreover, since blocking does depend on the choice of the alignment orientation, for each quasiparticle excitation reorientation effects should also be considered [4,8] retaining in each case the solution with the lowest energy. Therefore, to reduce the computational cost, in practical applications it is convenient to preserve time reversal as self-consistent symmetry. This was traditionally accomplished within the so called equal filling approximation (EFA), according to which the odd nucleon is half into a given orbital and half into its time-reversed partner. The microscopic justification of the EFA is based on standard ideas of quantum statistical mechanics and was considered in Ref. [3]. The predictions arising from various treatments of blocking have been compared in Ref. [4]. On one hand, it was shown that both exact blocking and EFA approach are strictly equivalent when the time-odd fields of the EDF are neglected. On the other hand, it was also concluded that the EFA is sufficiently precise for most practical applications. The EFA is precisely theapproximation employed in the present work to study the systematics of the ground and low-lying one-quasineutron states in odd-A nuclei with proton (neutron) numbers $38 \leqslant Z \leqslant 42$ ($47 \leqslant N \leqslant 67$).

The local systematics of one-quasiparticle excitations have already been studied in various mass regions either from macroscopic-microscopic approaches [9–12] or from the EDF theory [4,13–18]. To the best of our knowledge, still the only global study of odd nuclei within the nuclear EDF framework was reported in Ref. [2] where Skyrme-HF + BCS predictions for ground-state spins and parities have been compared with finite-range droplet model results.

As already mentioned, in this work we study neutron-rich Sr, Zr, and Mo odd isotopes with mass numbers $A \sim 100$. Nuclei in this region of the nuclear chart are being actively studied both theoretically [19–22] and experimentally [23–30] because of their interest from the nuclear structure perspective, as well as because of their significance in nuclear astrophysics. In particular, their masses and decay properties are an essential input to model the path, the isotopic abundances and the time scale of the r process in a reliable way [31]. In addition, this region is also characterized by the strong competition between various shapes, giving rise to shape instabilities that lead to shape coexistence and sudden shape transitions [21,32]. Thus, it is interesting to explore the predictive power of the Gogny-EDF [33] when applied to describe the ground and low-lying one-quasineutron states in odd-A nuclear systems belonging to this region. Although it is clear that one cannot expect *a priori* to reproduce in detail spectroscopic properties of the considered odd-A nuclei from global EDFs (see, e.g., [34–36]) the question still remains about the ability of the Gogny-type EDFs to describe, at least qualitatively, the main features of the observed trends in the Sr, Zr, and Mo isotopic chains.

In addition to D1S [37], which is the most standard and thoroughly tested parameter set (see, e.g., [38–53] and references therein), in the present study we have also considered the most recent parametrization of the Gogny-EDF, namely the D1M [54] parametrization. The goal is twofold. First we want to verify the robustness of our predictions with respect to the particular version of the EDF employed. If the results with two different EDFs (or two parametrizations of one, as

*luis.robledo@uam.es

is our case) are similar, we can be rather confident about the independence of the predictions with respect to the details of the EDF. The second goal is to test the performance of D1M in the present context (spectroscopy of odd-A nuclei) as to add arguments to decide whether D1M [54] can supersede the rather old D1S [37] parametrization or not. The fitting protocol of D1M includes input from a realistic equation of state (EoS) both in symmetric and neutron nuclear matter. It also explores, in the symmetric nuclear matter EoS case, the four possible spin-isospin channels and tries to reproduce the trends obtained in realistic Brueckner-Hartree-Fock calculations. As a consequence, the D1M parametrization reproduces the correct sign for the isovector splitting of the effective mass for neutron-rich matter at all possible asymmetries. The consequence of such a sophisticated fitting protocol is an energy root-mean-square deviation for the experimentally known 2149 masses of only 0.8 MeV, which is much better than the one of D1S. The systematic comparison [54] of the collective 2^+ excitation energies obtained with D1S and D1M (only even-even nuclei were considered) suggests that the later essentially keeps the same nuclear structure predictive power of the former. Subsequent analysis centered on the structure of the intrinsic wave functions [55] has confirmed the previous findings. Therefore, it is timely and necessary to further extend the comparison between D1S and D1M to odd nuclei. To this end, we analyze in the present paper the spectroscopic properties of neutron-rich Sr, Zr, and Mo odd isotopes in the $A \sim 100$ mass region within the Hartree-Fock-Bogoliubov (HFB) [7] plus EFA framework [3] (HFB-EFA). The election of the considered nuclei is mainly driven by the intense experimental [23–29] and theoretical [19–22] efforts to better characterize the structural evolution of the ground and excited nuclear shapes in this region of the nuclear chart [56].

The paper is organized as follows. In Sec. II, we present a brief description of the theoretical formalism used in the present work (i.e., the HFB-EFA framework). The results of our calculations for the considered nuclei are discussed in Sec. III where we pay attention to mean-field potential energy curves (PECs), equilibrium deformations of the various competing shapes, single-particle energies, one-quasineutron states, and their spectroscopic evolution along the Sr, Zr, and Mo isotopic chains. We also compare our results with the available experimental data. Finally, Sec. IV is devoted to the concluding remarks and work perspectives.

II. THEORETICAL FRAMEWORK

In the present study several Sr, Zr, and Mo isotopes with odd neutron number are studied. Nevertheless, the blocking procedure changing the number parity [6,7] of a given even-even HFB vacuum and providing us with the corresponding ground and low-lying one-quasiparticle states in odd-A nuclei also requires to consider even-A nuclei in these isotopic chains, as discussed below.

In previous studies of even-even nuclei we have found advantageous to use the so-called gradient method [55,57,58] to obtain the solution of the HFB equations, leading to the (even number parity) vacuum $|\Phi\rangle$. Within this method, the HFB equation is recast in terms of a minimization (variational) process of the mean-field energy and the Thouless parameters defining the most general HFB wave functions [7] are used as variational parameters. For a given point in the multidimensional variational space of the Thouless parameters the procedure uses the direction of the gradient in its search for the minimum. The advantage of the gradient method over others, like the successive iteration method, relies on the way constraints are implemented, which allows a larger number of them to be treated at once. As it is customary in calculations with the Gogny force, the kinetic energy of the center-of-mass motion was subtracted from the Routhian to be minimized to ensure that the center of mass is kept at rest. The exchange Coulomb energy was considered in the Slater approximation and we neglected the contribution of the Coulomb interaction to the pairing field. Both axial and time reversal are self-consistent symmetries in our calculations.

The quasiparticle creation and annihilation operators ($\hat{\beta}_k^\dagger$ and $\hat{\beta}_k$) associated with a given (even-even) HFB vacuum $|\Phi\rangle$ have been expanded in an axially symmetric harmonic oscillator (HO) basis ($\hat{c}_l^\dagger, \hat{c}_l$),

$$\begin{aligned} \beta_\mu^+ &= \sum_m U_{m\mu} c_m^+ + V_{m\mu} c_m, \\ \beta_\mu &= \sum_m U_{m\mu}^* c_m + V_{m\mu}^* c_m^+, \end{aligned} \tag{1}$$

containing enough number of shells (13 major shells) to grant convergence for all values considered of the mass quadrupole moment $Q_{20} = \frac{1}{2}\langle\Phi|2z^2 - x^2 - y^2|\Phi\rangle$ [58] and for all the nuclei studied.

Constrained calculations have been performed to generate PECs for even-even Sr, Zr, and Mo nuclei. Such PECs are displayed in Fig. 1 for a set of representative isotopes and the parametrization Gogny-D1S. One can also find a systematic compilation of PECs obtained with Gogny-D1S in Ref. [59]. The computation of such PECs is twofold: First, they give us initial hints on the evolution of the different competing shapes in the considered nuclei and, second, they provide a whole set of prolate, spherical, and oblate (reference) even-even HFB states for the subsequent treatment of the neighboring odd-N nuclei.

In fact, once a reference (even-even) state with a given deformation is chosen, we use it to perform an additional (constrained) HFB calculation providing an unblocked fully paired state corresponding to an odd average neutron number (false vacuum [1]) with the same deformation. Such prolate, spherical, and oblate false vacua are then used as input configurations in our subsequent blocking scheme (i.e., EFA).

The HFB ground-state wave function $|\Phi\rangle$ of an even-even nucleus is defined by the condition of being the vacuum of the annihilation quasiparticle operators β_μ defined in Eq. (1). Regarding observables (mean values) the HFB ground state of an even-even system is specified [7] by the (Hermitian) density matrix,

$$\rho_{ij} = (V^* V^T)_{ij}, \tag{2}$$

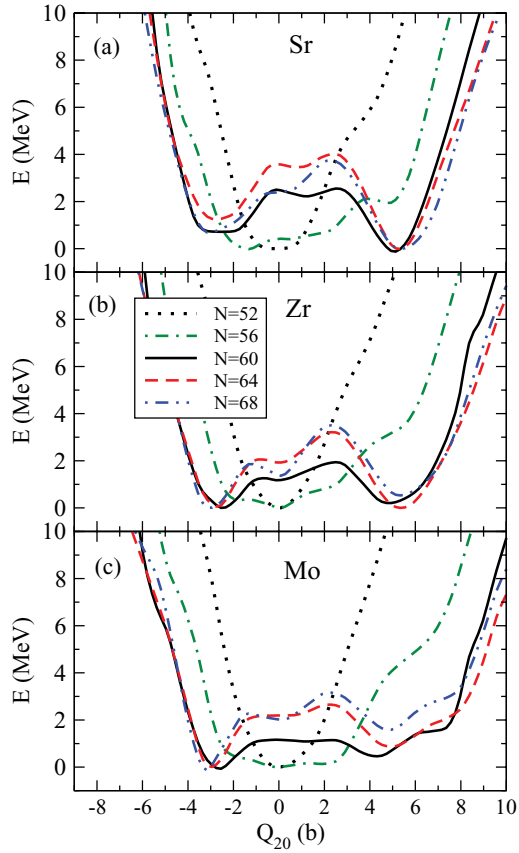

FIG. 1. (Color online) PECs for Sr (a), Zr (b), and Mo (c) isotopes with $N = 52, 56, 60, 64$, and 68 obtained from HFB calculations with the Gogny-D1S energy density functional.

and the (antisymmetric) pairing tensor,

$$\kappa_{ij} = (V^* U^T)_{ij}, \tag{3}$$

where the U and V amplitudes are those of Eq. (1) defining the Bogoliubov transformation. Applying any unitary transformation to the right of both amplitudes U and V leaves both ρ and κ (and therefore any mean value) unaltered whereas the quasiparticle operators are affected by the representation of the unitary transformation in operator space. This invariance is not maintained in the odd-A case, as we will discuss below, implying conceptual changes in the treatment of an odd-A system as compared to the simpler even-even case.

On the other hand, the ground and low-lying one-quasiparticle states of odd-A systems, like the ones considered in the present work, can be handled with blocked (odd number parity [6,7]) HFB wave functions,

$$|\Psi_{\mu_B}\rangle = \beta^+_{\mu_B}|\Phi\rangle, \tag{4}$$

where μ_B indicates the quasiparticle state to be blocked and stands for the indexes compatible with the symmetries of the odd nuclei, such as the angular momentum projection K and parity in the case of axial symmetry. In practice, the blocked state (4) can be accomplished by exchanging the columns labeled by the index μ_B in the HFB amplitudes U and V [see Eq. (1)] with the same columns in the matrices V^* and U^*, respectively [6,7,60].

The density matrix and the pairing tensor corresponding to the one-quasiparticle state (4), read

$$\begin{aligned}\rho_{ij}^{(\mu_B)} &= \langle\Psi_{\mu_B}|c_j^+ c_i|\Psi_{\mu_B}\rangle = \langle\Phi|\beta_{\mu_B} c_j^+ c_i \beta^\dagger_{\mu_B}|\Phi\rangle \\ &= (V^* V^T)_{ij} + (U^*_{j\mu_B} U_{i\mu_B} - V_{j\mu_B} V^*_{i\mu_B}),\end{aligned} \tag{5}$$

and

$$\begin{aligned}\kappa_{ij}^{(\mu_B)} &= \langle\Psi_{\mu_B}|c_j c_i|\Psi_{\mu_B}\rangle = \langle\Phi|\beta_{\mu_B} c_j c_i \beta^\dagger_{\mu_B}|\Phi\rangle \\ &= (V^* U^T)_{ij} + (U_{i\mu_B} V^*_{j\mu_B} - U_{j\mu_B} V^*_{i\mu_B}).\end{aligned} \tag{6}$$

They violate time-reversal invariance and so do the HF and pairing fields associated with them, making the numerical calculation much more difficult than in the even-even case. These matrices are no longer invariant under unitary transformations of the U and V amplitudes applied to their right. As a consequence, that degree of freedom has to be taken into account in the solution of the HFB equations. A manifestation of this effect is the reorientation effect [4,8] discussed recently.

A very useful approximation to (exact) blocking preserving time-reversal invariance is the EFA [3,4], where one writes the density matrix,

$$\begin{aligned}\rho_{ij}^{(\mathrm{EFA},\mu_B)} &= \tfrac{1}{2}(\langle\Phi|\beta_{\mu_B} c_j^\dagger c_i \beta^\dagger_{\mu_B}|\Phi\rangle + \langle\Phi|\beta_{\overline{\mu}_B} c_j^\dagger c_i \beta^\dagger_{\overline{\mu}_B}|\Phi\rangle) \\ &= (V^* V^T)_{ij} + \tfrac{1}{2}(U_{i\mu_B} U^*_{j\mu_B} - V^*_{i\mu_B} V_{j\mu_B}) \\ &\quad + \tfrac{1}{2}(U_{i\overline{\mu}_B} U^*_{j\overline{\mu}_B} - V^*_{i\overline{\mu}_B} V_{j\overline{\mu}_B}),\end{aligned} \tag{7}$$

and the pairing tensor,

$$\begin{aligned}\kappa_{ij}^{(\mathrm{EFA},\mu_B)} &= \tfrac{1}{2}(\langle\Phi|\beta_{\mu_B} c_j c_i \beta^\dagger_{\mu_B}|\Phi\rangle + \langle\Phi|\beta_{\overline{\mu}_B} c_j c_i \beta^\dagger_{\overline{\mu}_B}|\Phi\rangle) \\ &= (V^* U^T)_{ij} + \tfrac{1}{2}(U_{i\mu_B} V^*_{j\mu_B} - V^*_{i\mu_B} U_{j\mu_B}) \\ &\quad + \tfrac{1}{2}(U_{i\overline{\mu}_B} V^*_{j\overline{\mu}_B} - V^*_{i\overline{\mu}_B} U_{j\overline{\mu}_B}),\end{aligned} \tag{8}$$

including not only the μ_B state but also its time-reversed partner $\overline{\mu}_B$. The corresponding HF and pairing fields read

$$\Gamma_{ij}^{(\mathrm{EFA},\mu_B)} = \sum_{qp} \overline{v}_{iqjp} \rho_{pq}^{(\mathrm{EFA},\mu_B)}, \tag{9}$$

$$\Delta_{ij}^{(\mathrm{EFA},\mu_B)} = \frac{1}{2} \sum_{qp} \overline{v}_{ijqp} \kappa_{pq}^{(\mathrm{EFA},\mu_B)}, \tag{10}$$

and the total EFA energy can be written in the usual HFB form,

$$\begin{aligned}E^{(\mathrm{EFA},\mu_B)} &= \mathrm{Tr}[t\rho^{(\mathrm{EFA},\mu_B)}] + \tfrac{1}{2}\mathrm{Tr}[\Gamma^{(\mathrm{EFA},\mu_B)}\rho^{(\mathrm{EFA},\mu_B)}] \\ &\quad - \tfrac{1}{2}\mathrm{Tr}[\Delta^{(\mathrm{EFA},\mu_B)}\kappa^{(\mathrm{EFA},\mu_B)*}].\end{aligned} \tag{11}$$

The microscopic justification of this expression for $E^{(\mathrm{EFA},\mu_B)}$ was first given in Ref. [3] using ideas of quantum statistical mechanics. The EFA energy can be obtained as the statistical average, with a given density matrix operator, and applying the variational principle to it, the usual HFB-EFA equation [3] is obtained. The existence of a variational principle allows one to use the gradient method to solve the HFB-EFA equation [3] with the subsequent simplification in the treatment of the constraints.

The solution of the HFB-EFA (as well as the exact blocked HFB) equation depends upon the initial blocked level μ_B. In the HFB-EFA case, the K quantum number is self-consistently preserved along the calculation and so does the parity if octupole correlations are not allowed in the iterative process.

Blocking levels with different K values and parities lead to different quantum states of the odd-A nucleus, the ground state being the one with the lowest energy. Given a K value and parity, one could naively think that considering the quasiparticle with the lowest quasiparticle energy as the initial blocked level should lead to the lowest energy solution for that value of K and parity. However, because of the self-consistent nature of the whole process this is not by any means guaranteed and therefore several quasiparticles, usually corresponding to the lowest quasiparticle energies have to be considered. In addition, in the present case and owing to the presence of coexisting prolate, oblate, and spherical minima in some of the nuclei considered, blocked configurations with those quadrupole deformations have to be explored. For this reason the minimization process has to be carried out several times using different initial prolate, spherical, and oblate (false) vacua. We have repeated each calculation, for a given false vacuum and K values from $1/2$ up to $15/2$, using as initial blocking states the 12 quasiparticles corresponding to the lowest quasiparticle energies. The use of so many initial configurations is to make sure we are not going to miss the true ground state and all the lowest excited states. The resulting computational cost is high as in the worst case (three false vacua) we have to carry out for each nucleus a total of $8 \times 3 \times 12 = 288$ HFB-EFA calculations. Among all the resulting one-quasineutron configurations, we have selected those within a 1-MeV energy window and compare them with available experimental data (see, e.g., Figs. 3–5). Note that for nuclei in this region of the nuclear chart, there exist several competing shapes at low excitation energy and therefore our procedure assures that the lowest energy solution can be reached for all values of the quadrupole moment Q_{20} and mass number. Finally, let us also mention that in those cases where the neutron pairing energy of a given false vacuum is too small, we increase it by constraining the mean value of the number particle fluctuation neutron operator $(\Delta N)^2$ in this false vacuum. We have found that this procedure leads to a very fast convergence of the calculations.

III. RESULTS

A. Potential energy curves and single-particle energies

It was shown experimentally that the ground states of even-even Sr, Zr, and Mo isotopes with N ranging from the magic neutron number $N = 50$ up to $N \sim 60$ are weakly deformed, but they undergo a shape transition from nearly spherical to well-deformed prolate (oblate) configurations as $N = 60$ is approached and crossed. Evidence for such an abrupt shape-phase transition includes 2^+ lifetime measurements [24,28] and quadrupole moments for rotational bands [25], as well as isotopic shifts in nuclear charge radii [23,26,29]. Heavier Sr and Zr ($A \sim 110$) isotopes exhibit axially symmetric well-deformed shapes, whereas the heavier Mo isotopes display a tendency toward triaxiality [21,27]. Above this region, it was suggested [61] that the $N = 82$ shell closure might be quenched far from stability but still weak experimental evidence was found.

In Fig. 1, we show the PECs for the even-even Sr (a), Zr (b), and Mo (c) isotopes. We display PECs corresponding to N =52, 56, 60, 64, and 68 isotones from which, the main features of the shape evolution can be followed. Nuclei with $N = 52$ show a sharp spherical minimum that becomes rather shallow at $N = 56$. Isotopes with $N = 60$ are already deformed with oblate and prolate minima very close in energy. In the case of Sr isotopes the ground state is prolate, for Zr isotopes oblate and prolate minima are almost degenerate, whereas the ground state becomes oblate for Mo nuclei. For neutron numbers greater than 60, prolate and oblate minima become well defined. Our results agree well with the shape-phase change predicted around $N = 60$ by microscopic-macroscopic models [19,20,62,63] and microscopic self-consistent relativistic [64] and nonrelativistic [53,65] mean-field calculations. Later on, in Sec. III B, our analysis of the shape evolution in even-even Sr, Zr, and Mo nuclei will be further extended with the systematics of the ground and low-lying one-quasineutron configurations predicted by our HFB-EFA calculations for odd-A nuclei in these isotopic chains.

Another interesting outcome of our HFB calculations for even-even nuclei (see also the discussion in Sec. III B) are the proton and neutron single-particle energies (SPEs) shown in Fig. 2, as functions of the axial quadrupole moment Q_{20}, for the case of ^{102}Zr (Z =40, N =62). To obtain these Nilsson-like diagrams, we have computed the eigenvalues of the Routhian $h = t + \Gamma - \lambda_{20} Q_{20}$, with t being the kinetic energy operator, Γ the Hartree-Fock field, and $\lambda_{20} Q_{20}$ the term containing the Lagrange multiplier used to enforce the corresponding quadrupole constraint. Obviously, the usual mean-field constraints [7] on both neutron and proton numbers are also taken into account. Fermi levels are plotted with thick dashed (red) lines in the figure. These type of diagrams help us [55,58] to identify regions of low-level density around the corresponding Fermi levels which, according to the Jahn-Teller effect [66], favor the onset of deformation.

For axially symmetric configurations, the SPE levels are tagged by the (half integer) K quantum number that corresponds to the third component of the angular momentum in the intrinsic frame. Because of the time-reversal invariance, single-particle orbitals with the same absolute K value are degenerate (Kramers degeneracy). Positive (negative) parity levels are plotted with solid (dashed) lines. At the spherical configuration $Q_{20} = 0$, the quantum numbers nlj are recovered. The asymptotic quantum numbers $[N, n_z, \Lambda]K^\pi$ are shown in Fig. 2 for Q_{20} values close to those where the minima of the PECs (see Fig. 1) are located (vertical arrows). For each single-particle state they have been assigned according to the largest amplitude in the expansion of the single-particle wave function in the axially symmetric harmonic oscillator basis.

For the neutron-rich $A \sim 100$ nuclei of our concern in the present work, the valence protons occupy the $N = 3$ shell and start to fill the $g_{9/2}$ orbitals in the $N = 4$ shell. Neutrons occupy states belonging to the $N = 4$ shell, which are strongly mixed by deformation, and begin to fill the $h_{11/2}$ intruder orbitals coming down from the $N = 5$ oscillator shell. Because of their opposite parity, the $h_{11/2}$ neutron states (the $g_{9/2}$ proton states) do not mix with the $N = 4$ neutron orbitals (the $N = 3$ proton orbitals). These intruder orbitals polarize the core

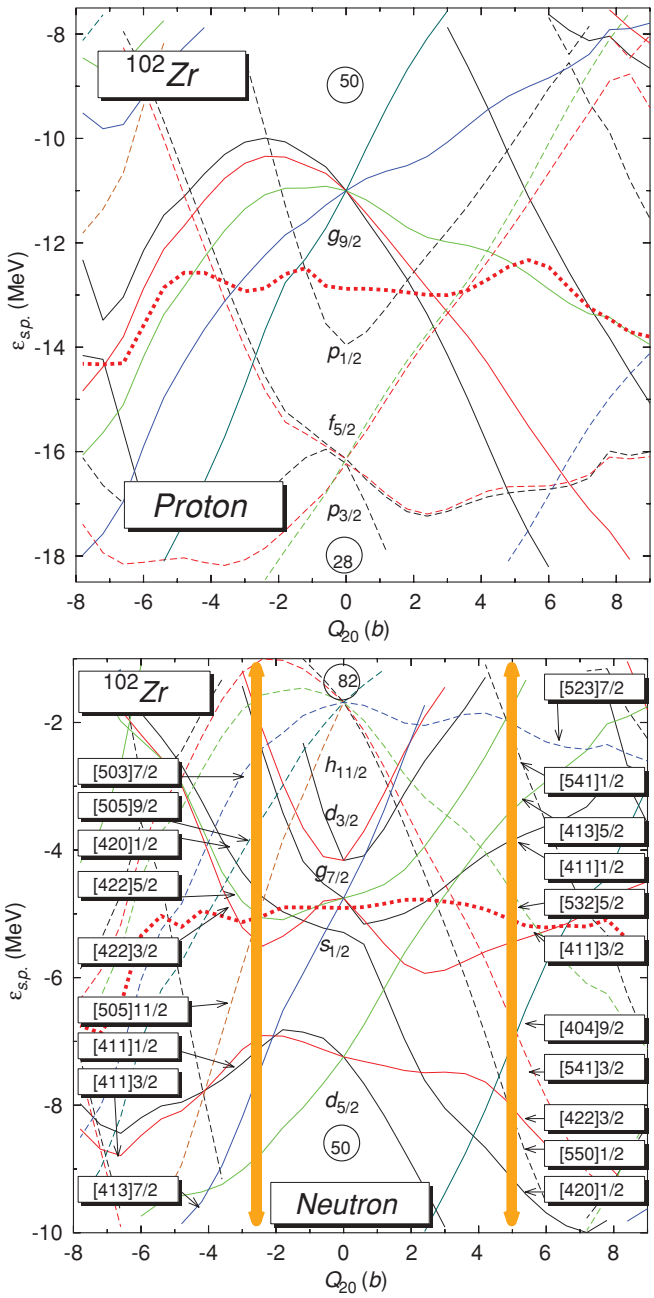

FIG. 2. (Color online) Single-particle energies for protons and neutrons in ^{102}Zr as a function of the axial quadrupole moment Q_{20}. The Fermi level is depicted as a thick dashed red line. The results have been obtained with the Gogny-D1S EDF. Solid lines correspond to levels with positive parity whereas dashed lines correspond to negative parity states. Asymptotic (Nilsson) quantum numbers $[N, n_z, \Lambda]K^\pi$ are shown in the neutron case for Q_{20} values close to those where the minima of the PECs are located (vertical arrows).

toward oblate and prolate deformations. As a consequence, the underlying nuclear structure in this mass region is very sensitive to the occupancy of these single-particle orbitals and the result is a rapid change in nuclear spectroscopic properties as a function of both neutron and proton numbers.

Below we compare the results obtained with the D1S parametrization of the force with those obtained with the newly introduced D1M parametrization. As it turns out that the spin orbit strength of D1M is 12% smaller than the one of D1S one may wonder whether this difference could lead to a strong impact in the single-particle spectrum and its behavior with deformation. To answer this question we have plotted the D1M single-particle levels and compared them to the D1S ones. The comparison of the two sets of levels shows small differences in the position of the levels (of the order of a few hundred of keV at most) that are not strong enough as to change the ordering of the spherical single-particle spectrum. The behavior with deformation is not changed in a significant way either. This small impact can be related to the larger effective mass of D1M as compared to D1S, which makes the single-particle spectrum more dense in D1M than in D1S. As a consequence a weaker spin-orbit strength is required in D1M to shift the intruders to the lower shell.

B. One-quasiparticle states in odd-*N* Sr, Zr, and Mo nuclei

In Figs. 3–5 results are given for odd-N Sr, Zr, and Mo isotopes, respectively. In each figure the experimental [56] ground and low-lying one-quasineutron states, characterized by their

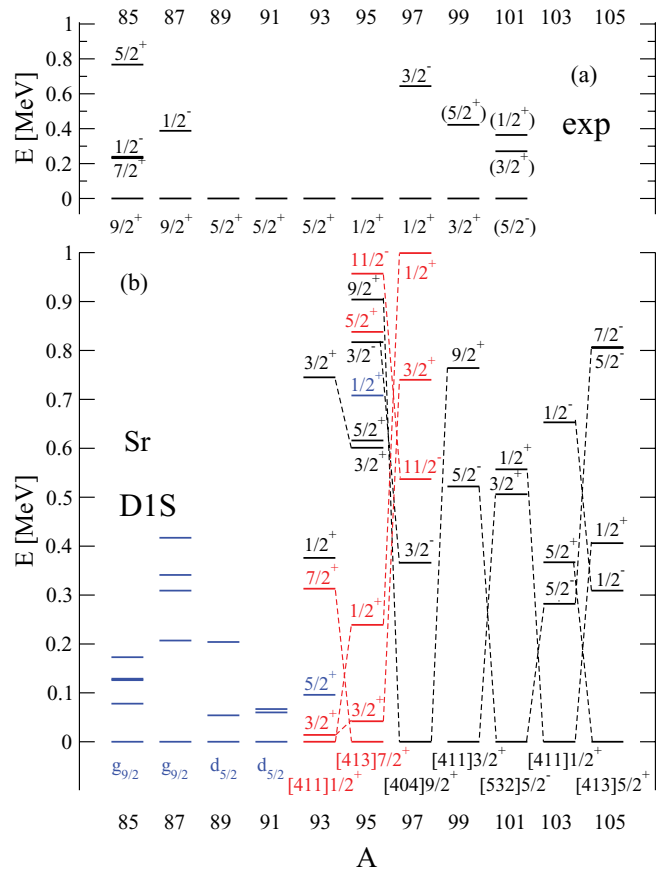

FIG. 3. (Color online) Experimental (a) excitation energies and spin-parity assignments of the noncollective states are compared with HFB-EFA results (b) for the one-quasineutron states in odd-N Sr isotopes (see text for details). Prolate configurations are shown by black lines, oblate ones by red lines, and spherical ones by blue lines.

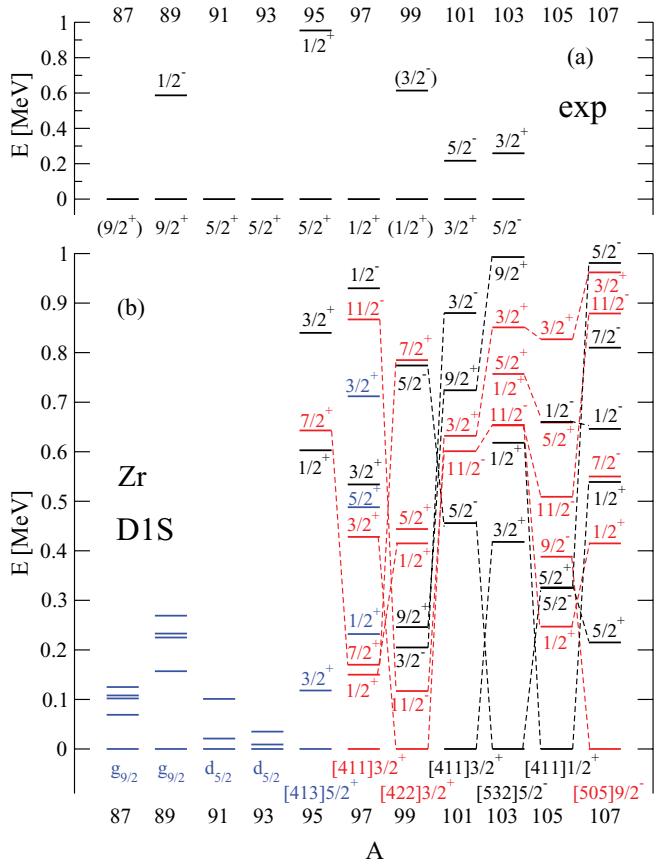

FIG. 4. (Color online) Same as in Fig. 3, but for odd-N Zr isotopes.

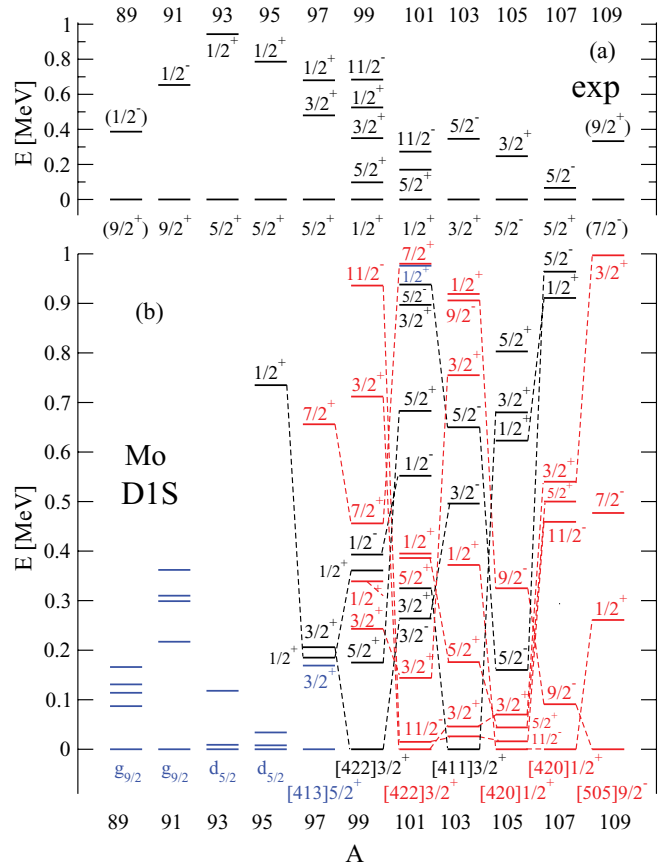

FIG. 5. (Color online) Same as in Fig. 3, but for odd-N Mo isotopes.

spin-parity assignments [(a) in the figures] are compared with the ones predicted within our HFB-EFA calculations [(b) in the figures]. This is certainly a very challenging test for the spectroscopic quality of the Gogny-D1S EDF for which results are shown. It is worth noting that in some cases the experimental spin and parity assignments in the (a) panels have been deduced from systematics and should be treated with caution.

The existence of oblate and prolate competing shapes in this mass region prevents us from using the usual convention [9,67] of plotting the theoretical results with hole (particle) states below (above) the corresponding ground state. In Figs. 3–5, the excited states in a given isotope are referred to the corresponding ground state regardless its shape. Prolate configurations are shown by black lines, oblate ones by red lines, and spherical ones by blue lines. The quasiparticle states in the deformed configurations are labeled by their K^π quantum numbers and, in addition, the ground states are labeled by their asymptotic (Nilsson) quantum numbers $[N, n_z, \Lambda]K^\pi$. In the lighter isotopes we obtain spherical (sharp or shallow) equilibrium shapes and therefore only the spherical orbital, which is either $g_{9/2}$ or $d_{5/2}$ in all the cases, is indicated. Like orbitals in neighbor isotopes are connected by dashed lines to better appreciate their isotopic evolution.

Looking at Figs. 3–5, the striking correlation between the ground-state deformations in the even-even isotopes (Fig. 1) and the ground-state shapes of the odd ones is observed. The lighter Sr nuclei ($A = 85$–91) are spherical. They become oblate for $A = 93$ and 95 with prolate states at low excitation energies. Finally, prolate deformed ground states are obtained in the heavier isotopes with $A = 97$–105. Oblate excited states below 1 MeV are obtained for $A = 97$, whereas they lie above 1 MeV in the heavier ones.

The lighter Zr isotopes ($A = 87$–95) displayed in Fig. 4, show spherical equilibrium shapes, which turn into oblate ($A = 97, 99$), prolate ($A = 101$–105), and again oblate ($A = 107$) ground states with excited one-quasiparticle configurations of different shapes below 1 MeV and very close in energy, in agreement with Fig. 1(b).

The odd Mo isotopes in Fig. 5 also display similarities with Fig. 1(c). Again, spherical ground states are found for the lighter isotopes. Alternating oblate and prolate equilibrium shapes are predicted in ^{99,101,103,105}Mo. Prolate and oblate configurations are particularly close in energy within this mass range. Oblate ground-state deformations are found for both ^{107,109}Mo with no prolate one-quasineutron configurations in ^{109}Mo below 1 MeV.

In Fig. 3, we compare the experimental (a) low-lying one-quasineutron spectra with the ones predicted by our HFB-EFA calculations (b) for odd-N Sr isotopes. We can see a reasonable agreement in the ground states, except for the isotopes ^{93,95,97}Sr. In ^{93}Sr, the $5/2^+$ experimental ground state appears at 0.1 MeV in our calculations, whereas in ^{95,97}Sr the $1/2^+$ experimental ground states are found as oblate

excited configurations at $E = 0.25$ and $E = 1$ MeV, respectively. The ground states of the heavier isotopes ^{99,101}Sr are well reproduced.

The structural evolution of the ground and excited one-quasiparticle states along the considered Sr, Zr, and Mo isotopic chains can also be followed by looking at the dashed lines connecting the states characterized by the same asymptotic quantum numbers $[N, n_z, \Lambda]K^\pi$ and at Fig. 2, as a guide. Indeed, the ground-state sequence as the number of neutron increases exhibits a clear correspondence with the orbitals found in Fig. 2 along thick vertical arrows at oblate ($Q_{20} \sim -2.5$ b) and prolate ($Q_{20} \sim 5$ b) quadrupole moments. For example, one sees how the ground state in ^{101}Sr, which corresponds to the prolate $[532]5/2^-$ state, becomes the first one-quasineutron excitation, below 0.6 MeV, in the neighboring ^{99}Sr and ^{103}Sr with prolate $[411]3/2^+$ and $[411]1/2^+$ ground states. On the other hand, ^{97}Sr exhibits a prolate $[404]9/2^+$ ground state, which turns out to be a quasineutron band head in ^{95}Sr and ^{99}Sr whereas the $[411]1/2^+$ prolate ground state in ^{103}Sr appears as an excited state between 0.6 and 0.4 MeV in ^{101}Sr and ^{105}Sr, respectively.

In Fig. 4 the comparison is made for Zr isotopes. The agreement is again a very reasonable exception made of ^{97,99}Zr for which the reported ground states appear in our HFB-EFA calculations as oblate excited states below 0.5 MeV. Special mention deserves, the remarkable agreement for the heavier isotopes ^{101,103}Zr, where our calculations reproduce both the ground states and the low-lying excitations. One can see, how the band head $5/2^-$ at 0.45 MeV in ^{101}Zr and the ground state in ^{103}Zr correspond to the same $[532]5/2^-$ single-particle configuration, as was experimentally established in Ref. [27].

The dashed lines in Fig. 4 are also useful to trace the isotopic evolution of the single-particle configurations, which can be also understood by moving the (neutron) Fermi level in Fig. 2 through the vertical arrows. Thus, taking, for example, the prolate solutions, if one looks at the orbitals intersecting the vertical arrow at $Q_{20} = 5$ b in Fig. 2, one finds the deepest state at about $e_{sp} = -9$ MeV, which corresponds to a $[420]1/2^+$ ($s_{1/2}$) state. It can be seen, in Fig. 4, as the prolate excited state at 0.6 MeV in ^{95}Zr. The next prolate states in Fig. 2 are $[550]1/2^-$ falling down very quickly from $h_{11/2}$ and $[422]3/2^+$ ($d_{5/2}$) appearing as the first prolate excitations in ^{97}Zr. On the other hand, in ^{99}Zr the first two prolate states $3/2^-$ and $9/2^+$ appear around 0.2 MeV. They are associated with the $[541]3/2^-$ coming down from $h_{11/2}$ and $[404]9/2^+$ raising from $g_{9/2}$ in Fig. 2. Going further up in Fig. 2 we find $[411]3/2^+$ ($g_{7/2}$), which is the ground state in ^{101}Zr and $[532]5/2^-$ ($h_{11/2}$) which represents an excited state at about 0.45 MeV. Further up in excitation energy one finds the $9/2^+$ and $3/2^-$ states already discussed (see the connections with dashed lines with their partners in ^{99}Zr). In ^{103}Zr the $3/2^+$ and $5/2^-$ states interchange their positions with respect to ^{101}Zr and, as it can be easily understood from Fig. 2, the $[532]5/2^-$ configuration becomes now the ground state. Subsequently, the $[411]1/2^+$ ($g_{7/2}$) ground state is predicted by our HFB-EFA. The excited one-quasineutron $5/2^-$ and $5/2^+$ states, at about 0.35 MeV, correspond to the already discussed $[532]5/2^-$ ($h_{11/2}$), which now lies below the Fermi level, and

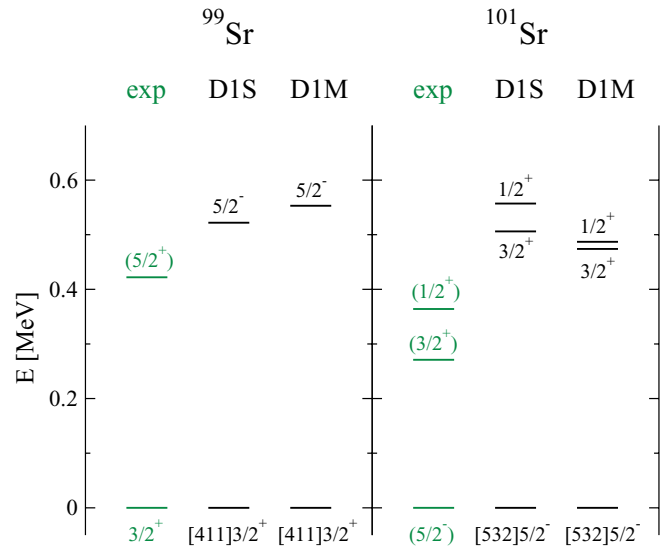

FIG. 6. (Color online) Excitation spectra of some Sr isotopes obtained within the HFB-EFA calculations based on the D1S and D1M parametrizations of the Gogny-EDF are compared with available experimental data. The color scheme used to characterize the quadrupole deformation of each of the states is the same as in Fig. 3. Experimental levels are plotted in green because there is no clear experimental evidence concerning the sign of their intrinsic deformations.

to the $[413]5/2^+$ ($d_{5/2}$) configuration, above the Fermi level, that becomes the lowest prolate deformed one-quasiparticle excitation in the last odd-N nucleus considered (i.e., ^{107}Zr).

A similar analysis can be made for the oblate one-quasineutron states by looking at the intersections of the single-particle levels in Fig. 2 with the vertical line at $Q_{20} = -2.5$ b. As can be seen from Fig. 4, ^{97}Zr displays a ground $3/2^+$ and two low-lying excited ($1/2^+$ and $7/2^+$) oblate deformed states. They can be associated with the three orbitals at -8 MeV in the oblate sector of Fig. 2, namely, $[411]3/2^+$ ($d_{5/2}$), $[411]1/2^+$ ($d_{5/2}$), and $[413]7/2^+$ ($g_{7/2}$). Next, in ^{99}Zr we find an oblate $3/2^+$ ground state and the oblate $11/2^-$ excitation at 0.1 MeV that correspond to the $[422]3/2^+$ ($g_{7/2}$) and $[505]11/2^-$ intruder state coming down from the $h_{11/2}$ shell. The $[420]1/2^+$ and $[422]5/2^+$ (coming from the $g_{7/2}$ shell) excitations, are also visible in the quasiparticle spectrum of ^{99}Zr. The nucleus ^{101}Zr exhibits a prolate ground state but one finds a $[505]11/2^-$ as the lowest oblate quasineutron configuration very close to the $3/2^+$ excitation (that was the ground state in ^{99}Zr). The same comments apply to both ^{103}Zr and ^{105}Zr but now the state $[420]1/2^+$ ($s_{1/2}$) comes into play. Finally, ^{107}Zr displays an oblate ground state that can be associated with a $[505]9/2^-$ configuration coming down from the $h_{11/2}$ shell.

According to the discussions in Ref. [27], where the rotational bands of the lowest quasiparticle states were measured, and the results of our recent study in Ref. [21], where triaxial shapes were predicted in neutron-rich Mo isotopes, the odd Mo nuclei are the most difficult to analyze. Our HFB-EFA description in terms of axial shapes nicely reproduces the ground $5/2^+$ and the two excited $3/2^+$ and $1/2^+$ states in ^{97}Mo.

Our calculations also provide us with the observed $1/2^+$, $5/2^+$, $3/2^+$, and $11/2^-$ one-quasiparticle configurations in ^{99}Mo although redistributed. The observed $1/2^+$, $5/2^+$, and $11/2^-$ states are obtained in ^{101}Mo within 0.4 MeV excitation energy. On the other hand, the ground state in ^{103}Mo is well reproduced whereas the excited $5/2^-$ appears at about 0.6 MeV. The latter becomes the experimental ground state in ^{105}Mo, but it is predicted at 0.15 MeV in our calculations. Finally, the observed ground states in both ^{107}Mo and ^{109}Mo are obtained as oblate excited (about 0.5 MeV) configurations within our HFB-EFA calculations.

In general, we observe that the main difficulties to describe the experimental information appear in those cases where the mean-field approach might not be sufficient. Such is the case of $N = 55$–59 isotopes, where we get very shallow minima (see Fig. 1), a situation that in general requires configuration mixing for a better description. Work along this direction has already been carried out in [68,69] in the context of a collective Hamiltonian obtained in the Gaussian overlap approximation (GOA) framework. We believe that a better treatment of the problem is required to pin down the subtle details of the spectrum of an odd-A system and therefore the exact generator coordinate method (GCM) with the axial quadrupole moment would be required. Work along this line is in progress and will be reported elsewhere. Difficulties also appear when the description requires the consideration of triaxility as it is the case for the heavier Mo isotopes, which exhibit a γ-soft behavior and even triaxial minima [21] with the axial ones converted into saddle points. In such a situation one also expects that the oblate and prolate solutions will be highly mixed with the intermediate triaxial configurations. On the other hand, an HFB axial description is expected to work better for well-developed axial minima separated by energy barriers in both spherical and triaxial shapes as in the heavier isotopes of Sr and Zr.

Another interesting point worth noticing is the isotonic behavior of the considered odd-A nuclei. Because the isotopes studied in this work have an odd number of neutrons, one observes very similar spectroscopic schemes for fixed number of neutrons (isotones), where the odd neutron determines the spin and parity of the ground state. First, one realizes the observed experimental correspondence between the spins and parities of isotones within Sr, Zr, and Mo nuclei. Thus, starting at $N = 47$ with $J^\pi = 9/2^+$ in ^{85}Sr, ^{87}Zr, and ^{89}Mo, the sequence of $9/2^+$, $9/2^+$, $5/2^+$, $5/2^+$, $5/2^+$, $1/2^+$, $1/2^+$, $3/2^+$, $5/2^-$ is observed experimentally from $N = 47$ up to $N = 63$. The agreement between these experimental findings and our calculations is specially remarkable in the heavier isotones.

For $N = 61$ (^{99}Sr, ^{101}Zr, ^{103}Mo) the ground state corresponds to $[411]3/2^+$ states both experimentally and theoretically. In addition, a low-lying band head $5/2^-$ is observed experimentally [27] in ^{101}Zr and ^{103}Mo that corresponds reasonably well with the predictions of our HFB-EFA calculations. The experimental assignment $(5/2^+)$ to the excited state in ^{99}Sr is uncertain and could also correspond to a $5/2^-$ in which case the similarity would be complete. The $N = 63$ isotones ^{101}Sr and ^{103}Zr exhibit a $[532]5/2^-$ ground state in agreement with experiment. In the case of ^{105}Mo

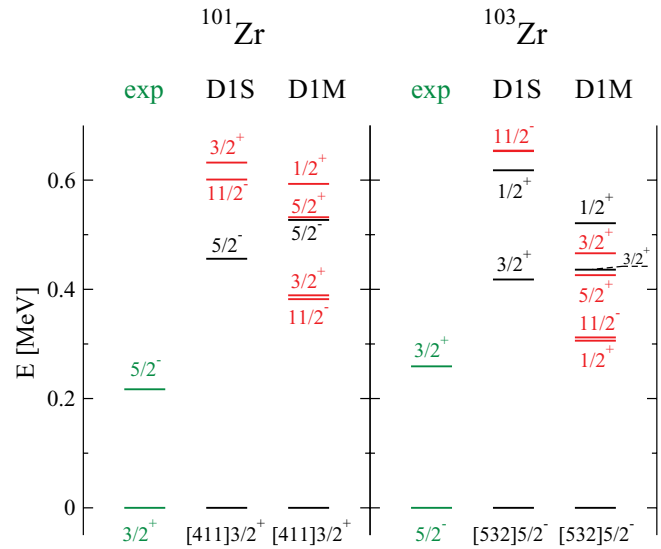

FIG. 7. (Color online) Same as in Fig. 6, but for Zr isotopes.

we obtain an oblate ground state $[420]1/2^+$, which does not show up experimentally, but the first excited prolate state is again $[532]5/2^-$. Excited $3/2^+$ quasiparticle configurations observed experimentally at $N = 63$ are also well reproduced in the calculations as prolate configurations. The $N = 65$ isotones ^{103}Sr and ^{105}Zr are predicted to be prolate $[411]1/2^+$ in their ground states, whereas ^{107}Mo is predicted as an oblate $[420]1/2^+$ at variance with experiment.

The main difficulty in understandering the previous correspondence appears in the isotones $N = 57$, 59, where the experimental $1/2^+$ assignments to their ground states are difficult to reproduce in our calculations. However, these $1/2^+$ quasiparticle states appear in the calculations as excited oblate configurations at low excitation energies. The $3/2^-$ excited state observed experimentally in ^{97}Sr and ^{99}Zr appear in our calculations at similar energies as prolate configurations. In $^{99-101}$Mo there are two excited $5/2^+$ and $11/2^-$ states also found in our HFB-EFA calculations below the 1-MeV energy window of the plot.

As mentioned in Sec. I, one of our aims in the present study was to further extend the comparison, already undertaken in Ref. [55], between the performance of the parametrizations Gogny-D1S and Gogny-D1M to the description of the spectroscopy of odd-A nuclei. Therefore, in Fig. 6 (for ^{99,101}Sr), Fig. 7 (for ^{101,103}Zr), and Fig. 8 (for ^{103,105}Mo), we compare the results obtained for the low-lying one-quasineutron states using these two different incarnations of the Gogny-EDF with the experimental data. First, one realizes the nice similarity between the HFB-EFA predictions obtained with these two parametrizations. In particular, the predicted ground states coincide in most of the cases and agree well with experiment. Only in Mo isotopes one observes some disagreement but, in this case, we obtain a high density of very low-lying configurations with the observed ground states always below 0.2 MeV.

Looking at the figures in more detail, we can see that within the considered energy window of 0.7 MeV, practically the same states are obtained from the calculations with D1S and

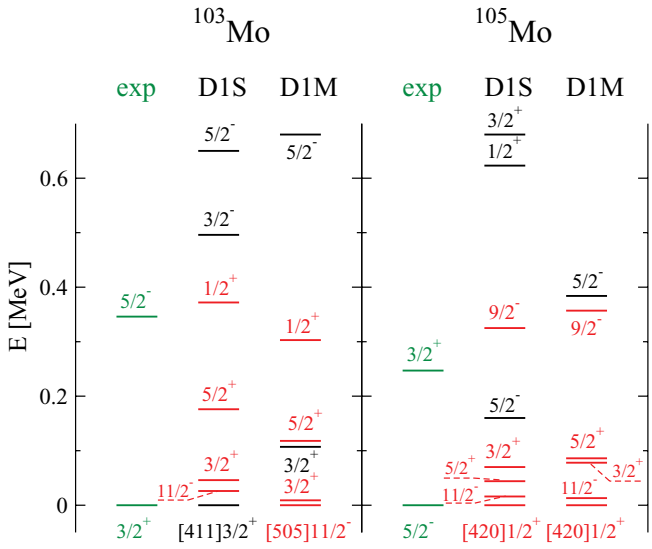

FIG. 8. (Color online) Same as in Fig. 6, but for Mo isotopes.

D1M. This is especially true for prolate deformed states. For example, in Sr isotopes (Fig. 6) we obtain the same $5/2^-$ states in ^{99}Sr as well as the $3/2^+$ and $1/2^+$ states in ^{101}Sr very close to the experiment and with very small variations (less than 0.2 MeV) from one EDF to another.

The same happens in Fig. 7 for the Zr isotopes. The prolate states $5/2^-$ (in ^{101}Zr) and $3/2^+$, $1/2^+$ (in ^{103}Zr) are predicted very close with D1S and D1M and agree well with experiment. However, we observe an enhanced sensitivity in the case of the oblate configurations, resulting in lower energies, of the order of a few hundred keV, in the case of D1M with respect to D1S. This is a consequence of having closer oblate and prolate minima with the parametrization D1M. The ground states are nicely reproduced.

In the case of Mo isotopes (Fig. 8) the experimental ground and first excited state are interchanged in ^{103}Mo and ^{105}Mo. Our HFB-EFA calculations provide prolate $3/2^+$ and $5/2^-$ states compatible with experiment, but also other oblate configurations at very low excitation energy. We can see $11/2^-$, $3/2^+$, $5/2^+$, and $1/2^+$ low-lying oblate states in ^{103}Mo. In addition to those, we also find an oblate $9/2^-$ state in ^{105}Mo. As for Zr isotopes, we also find that D1M tends to favor oblate solutions, which appear displaced to lower energies with respect to the prolate solutions in D1S. In general we obtain a comparable spectroscopic quality of the two Gogny parametrizations and it is very satisfying to observe how the new parametrization D1M, in spite of the relaxation of some of the original constraints in its fitting protocol and the fact that it is more oriented to reproducing nuclear masses [54], still follows very closely the fine details predicted with Gogny-D1S for odd-A nuclei in a region of the nuclear chart with such a challenging shape evolution.

IV. CONCLUSIONS

In this work we have studied the systematics of one-quasineutron configurations in odd-A Sr, Zr, and Mo isotopes within the selfconsistent HFB plus EFA framework, an approach that was shown to be fairly adequate for most purposes. However, we are aware of the challenge of reproducing in detail the observed spectroscopic properties in the particular mass region considered in the present study. Therefore, our aim was to understand qualitatively the structural evolution of the ground and low-lying one-quasiparticle configurations with neutron number. We have also shown that the quality of the spectroscopic results obtained with the recent D1M parametrization of the Gogny force is comparable to the one obtained with the standard parametrization D1S. We conclude that both D1M and D1S parametrizations reproduce, at least qualitatively, the main features observed in the isotopic (and isotonic) trends of the neutron-rich and odd-A Sr, Zr, and Mo nuclei.

The main deficiency of our mean-field description is the preservation of axial symmetry. We have found this to be relevant in nuclei characterized by shallow minima around the spherical configurations like in the $N = 55$–59 isotopes, as well as in those nuclei with some tendency to γ-soft behavior or even triaxial minima like in the heavier Mo isotopes [21]. A beyond mean-field treatment seems to be necessary to improve the quality of the description in those cases, and configuration mixing calculations in the spirit of the generator-coordinate method (GCM) [7] may be required to improve the mean-field results. We are still far from being able to apply such a configuration mixing approach within an exact blocking scheme for odd nuclei. Nevertheless, a HFB-EFA-GCM scheme can be considered as a plausible step forward in this direction and work along this lines is in progress.

ACKNOWLEDGMENTS

This work was supported by Ministerio de Ciencia e Innovación (Spain) under research Grants No. FIS2008–01301, No. FPA2009-08958, and No. FIS2009-07277, as well as by Consolider-Ingenio 2010 Programs CPAN CSD2007-00042 and MULTIDARK CSD2009-00064. The first steps of this work were undertaken in the framework of the Finland Distinguished Professor Program (Academy of Finland and University of Jyväskylä). R.R. thanks Professors J. Dobaczewski and J. Äysto and the experimental teams of the University of Jyväskylä (Finland) for warm hospitality and encouraging discussions.

[1] T. Duguet, P. Bonche, P.-H. Heenen, and J. Meyer, Phys. Rev. C **65**, 014310 (2001).
[2] L. Bonneau, P. Quentin, and P. Möller, Phys. Rev. C **76**, 024320 (2007).
[3] S. Perez-Martin and L. M. Robledo, Phys. Rev. C **78**, 014304 (2008).
[4] N. Schunck, J. Dobaczewski, J. McDonnell, J. More, W. Nazarewicz, J. Sarich, and M. V. Stoitsov, Phys. Rev. C **81**, 024316 (2010).
[5] I. Hamamoto, Phys. Rev. C **79**, 014307 (2009).
[6] H. J. Mang, Phys. Rep. **18**, 325 (1975).

[7] P. Ring and P. Schuck, *The Nuclear Many-Body Problem* (Springer-Verlag, Berlin, 1980).
[8] P. Olbratowski, J. Dobaczewski, J. Dudek, and W. Plóciennik, Phys. Rev. Lett. **93**, 052501 (2004).
[9] W. Nazarewicz, M. A. Riley, and J. D. Garrett, Nucl. Phys. A **512**, 61 (1990).
[10] W. Ogle, S. Wahlborn, R. Piepenbring, and S. Fedriksson, Rev. Mod. Phys. **43**, 424 (1971).
[11] S. Ćwiok and W. Nazarewicz, Nucl. Phys. A **529**, 95 (1991).
[12] S. Ćwiok, S. Hofmann, and W. Nazarewicz, Nucl. Phys. A **573**, 356 (1994).
[13] K. Rutz, M. Bender, P.-G. Reinhard, J. A. Maruhn, and W. Greiner, Nucl. Phys. A **634**, 67 (1998).
[14] S. Ćwiok, W. Nazarewicz, and P. H. Heenen, Phys. Rev. Lett. **83**, 1108 (1999).
[15] W. Satula, R. A. Wyss, and M. Zalewski, Phys. Rev. C **78**, 011302(R) (2008).
[16] K. Rutz, M. Bender, P.-G. Reinhard, and J. A. Maruhn, Phys. Lett. B **468**, 1 (1999).
[17] A. V. Afanasjev, T. L. Khoo, S. Frauendorf, G. A. Lalazissis, and I. Ahmad, Phys. Rev. C **67**, 024309 (2003).
[18] A. V. Afanasjev and H. Abusara, Phys. Rev. C **81**, 014309 (2010).
[19] J. Skalski, S. Mizutori, and W. Nazarewicz, Nucl. Phys. A **617**, 282 (1997).
[20] F. R. Xu, P. M. Walker, and R. Wyss, Phys. Rev. C **65**, 021303(R) (2002).
[21] R. Rodríguez-Guzmán, P. Sarriguren, L. M. Robledo, and S. Perez-Martin, Phys. Lett. B **691**, 202 (2010).
[22] P. Sarriguren and J. Pereira, Phys. Rev. C **81**, 064314 (2010).
[23] F. Buchinger *et al.*, Phys. Rev. C **41**, 2883 (1990).
[24] H. Mach *et al.*, Nucl. Phys. A **523**, 197 (1991).
[25] W. Urban *et al.*, Nucl. Phys. A **689**, 605 (2001).
[26] P. Campbell *et al.*, Phys. Rev. Lett. **89**, 082501 (2002).
[27] H. Hua *et al.*, Phys. Rev. C **69**, 014317 (2004).
[28] C. Goodin *et al.*, Nucl. Phys. A **787**, 231c (2007).
[29] F. C. Charlwood *et al.*, Phys. Lett. B **674**, 23 (2009).
[30] J. Pereira *et al.*, Phys. Rev. C **79**, 035806 (2009).
[31] J. J. Cowan, F.-K. Thielemann, and J. W. Truran, Phys. Rep. **208**, 267 (1991).
[32] J. L. Wood, K. Heyde, W. Nazarewicz, M. Huyse, and P. Van Duppen, Phys. Rep. **215**, 101 (1992).
[33] J. Dechargé and D. Gogny, Phys. Rev. C **21**, 1568 (1980).
[34] M. Zalewski, J. Dobaczewski, W. Satula, and T. R. Werner, Phys. Rev. C **77**, 024316 (2008).
[35] M. V. Stoisov, J. Dobaczewski, W. Nazarewicz, and P. Borycki, Int. J. Mass Spectrom. **251**, 243 (2006).
[36] M. Kortelainen, J. Dobaczewski, K. Mizuyama, and J. Toivanen, Phys. Rev. C **77**, 064307 (2008).
[37] J. F. Berger, M. Girod, and D. Gogny, Nucl. Phys. A **428**, 23c (1984).
[38] L. M. Robledo, J. L. Egido, B. Nerlo-Pomorska, and K. Pomorski, Phys. Lett. B **201**, 409 (1988).
[39] J. L. Egido and L. M. Robledo, Nucl. Phys. A **545**, 589 (1992).
[40] J. L. Egido and L. M. Robledo, Phys. Rev. Lett. **70**, 2876 (1993).
[41] E. Garrote, J. L. Egido, and L. M. Robledo, Phys. Rev. Lett. **80**, 4398 (1998); Nucl. Phys. A **654**, 723c (1999).
[42] R. R. Rodríguez-Guzmán, J. L. Egido, and L. M. Robledo, Nucl. Phys. A **709**, 201 (2002).
[43] R. R. Rodríguez-Guzmán, J. L. Egido, and L. M. Robledo, Phys. Rev. C **65**, 024304 (2002).
[44] R. R. Rodríguez-Guzmán, J. L. Egido, and L. M. Robledo, Phys. Rev. C **69**, 054319 (2004).
[45] R. R. Rodríguez-Guzmán, J. L. Egido, and L. M. Robledo, Phys. Rev. C **62**, 054319 (2000).
[46] J. L. Egido, L. M. Robledo, and R. R. Rodríguez-Guzmán, Phys. Rev. Lett. **93**, 082502 (2004).
[47] J. F. Berger, M. Girod, and D. Gogny, Nucl. Phys. A **502**, 85c (1989).
[48] C. R. Chinn, J. F. Berger, D. Gogny, and M. S. Weiss, Phys. Rev. C **45**, 1700 (1992).
[49] M. Girod, J. P. Delaroche, D. Gogny, and J. F. Berger, Phys. Rev. Lett. **62**, 2452 (1989).
[50] G. F. Bertsch, M. Girod, S. Hilaire, J. P. Delaroche, H. Goutte, and S. Peru, Phys. Rev. Lett. **99**, 032502 (2007).
[51] S. Péru, J. F. Berger, and P. F. Bortignon, Eur. Phys. J. A **26**, 25 (2005).
[52] S. Hilaire and M. Girod, Eur. Phys. J. A **33**, 237 (2007).
[53] J.-P. Delaroche *et al.*, Phys. Rev. C **81**, 014303 (2010).
[54] S. Goriely, S. Hilaire, M. Girod, and S. Péru, Phys. Rev. Lett. **102**, 242501 (2009).
[55] R. Rodríguez-Guzmán, P. Sarriguren, L. M. Robledo, and J. E. García-Ramos, Phys. Rev. C **81**, 024310 (2010).
[56] Evaluated Nuclear Structure Data Files (ENSDF) [www.nndc.bnl.gov/ensdf].
[57] J. L. Egido, J. Lessing, V. Martin, and L. M. Robledo, Nucl. Phys. A **594**, 70 (1995).
[58] L. M. Robledo, R. Rodríguez-Guzmán, and P. Sarriguren, J. Phys. G: Nucl. Part. Phys. **36**, 115104 (2009).
[59] [www-phynu.cea.fr/science_en_ligne/carte_potentiels_microscopiques/carte_potentiel_nucleaire_eng.htm].
[60] B. Banerjee, H. J. Mang, and P. Ring, Nucl. Phys. A **215**, 366 (1976).
[61] J. Dobaczewski, W. Nazarewicz, T. R. Werner, J. F. Berger, C. R. Chinn, and J. Decharge, Phys. Rev. C **53**, 2809 (1996).
[62] P. Möller, J. R. Nix, W. D. Myers, and W. J. Swiatecki, At. Data Nucl. Data Tables **59**, 185 (1995).
[63] P. Möller *et al.*, At. Data Nucl. Data Tables **94**, 758 (2008).
[64] G. A. Lalazissis, S. Raman, and P. Ring, At. Data Nucl. Data Tables **71**, 1 (1999).
[65] M. Bender, G. F. Bertsch, and P.-H. Heenen, Phys. Rev. C **73**, 034322 (2006); **78**, 054312 (2008).
[66] P.-G. Reinhard and E. W. Otten, Nucl. Phys. A **420**, 173 (1984).
[67] B. S. Nielsen and M. E. Bunker, Nucl. Phys. A **245**, 376 (1975).
[68] N. Vermeulen *et al.*, Phys. Rev. C **75**, 051302(R) (2007).
[69] L. Gaudefroy *et al.*, Phys. Rev. Lett. **102**, 092501 (2009).